

The effects of native and modified clupeine on the structure of gram-negative model membranes

Article

Accepted Version

Creative Commons: Attribution-Noncommercial-No Derivative Works 4.0

English, M., Paulson, A., Green, R. J., Florek, O., Clifton, L. A., Arnold, T. and Frazier, R. A. (2019) The effects of native and modified clupeine on the structure of gram-negative model membranes. *Food Structure*, 22. 100127. ISSN 2213-3291 doi: <https://doi.org/10.1016/j.foostr.2019.100127> Available at <http://centaur.reading.ac.uk/86551/>

It is advisable to refer to the publisher's version if you intend to cite from the work. See [Guidance on citing](#).

To link to this article DOI: <http://dx.doi.org/10.1016/j.foostr.2019.100127>

Publisher: Elsevier

All outputs in CentAUR are protected by Intellectual Property Rights law, including copyright law. Copyright and IPR is retained by the creators or other copyright holders. Terms and conditions for use of this material are defined in

the [End User Agreement](#).

www.reading.ac.uk/centaur

CentAUR

Central Archive at the University of Reading

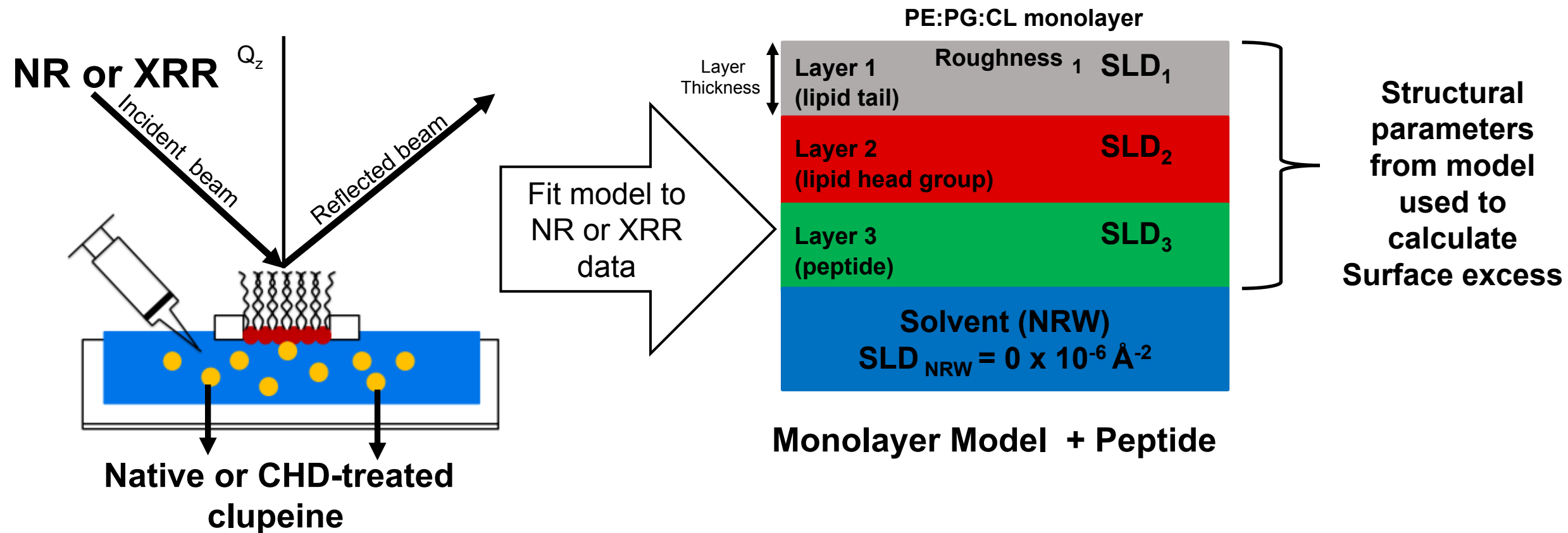
Reading's research outputs online

Highlights

- Similar structural effects were observed for both peptides in the monolayer and bilayer models, however, the magnitude of the effect was greater in the presence of the chemically modified peptide.
- Improved hydrophobicity and electrostatic interactions with lipid head groups resulting in thickening of the peptide layer, along with lipid translocation in the inner tail region of the bilayer, strongly suggests that the modified clupeine may use the carpet mechanisms to exert its effect on model membranes.
- Simultaneous fitting of neutron reflectometry and x-ray reflectometry data from PE:PG:CL monolayer model systems, resulted in quantitative determination of surface excess values for both native and modified clupeine.

Graphical Abstract

March 3, 2019



1 **Title:** The **effects** of native and modified clupeine on the **structure** of Gram-negative model
2 membranes.

3
4 **Name of authors:** M. English^a, A. Paulson^b, R. J. Green^c, O. Florek, L. A. Clifton^d, T. Arnold^e,
5 & R. A. Frazier^f.

6
7 **Contact information for corresponding author:** Marcia M. English, 2320 Notre Dame
8 Avenue, Antigonish, Nova Scotia, menglish@stfx.ca

9
10 **All other author affiliations**

11 ^aDepartment of Human Nutrition, Saint Francis Xavier University, Antigonish, Nova Scotia;

12 ^bDepartment of Process Engineering and Applied Science, Dalhousie University, Halifax, Nova
13 Nova Scotia, Canada.

14 ^cSchool of Pharmacy, University of Reading, Reading, PO Box 226, Whiteknights, Reading,
15 RG6 6AP, UK

16 ^dISIS, Science and Technology Facilities Council, Rutherford Appleton Laboratory, Didcot, UK

17 ^eEuropean Spallation Source, Lund, Sweden

18 ^fDepartment of Food and Nutritional Sciences, University of Reading, Reading, Harry Nursten
19 Building, PO Box 226, Whiteknights, Reading, RG6 6AP, UK

20
21
22 **Word count of text: “7,254 words”**

23
24 **Short version of title:** Structural effects of clupeine in model membranes.
25
26
27
28
29
30

31 **ABSTRACT:** Clupeine, a cationic antimicrobial peptide found in fish, is of interest as a food
32 additive but non-specific binding of the peptide to anionic molecules reduces its antimicrobial
33 activity. The overall positive charge of clupeine can be reduced by blocking 10% of its arginine
34 residues with 1,2-cyclohexanedione (CHD). The modified peptide retains antimicrobial activity
35 but it is not known if its effect on the structure of Gram-negative model membranes is the same as
36 the native peptide. In the presented paper, neutron reflectometry (NR) and X-ray reflectometry
37 were used to investigate the effect of native and modified clupeine on the structure of model
38 monolayer membranes composed of Phosphatidylethanolamine (PE), Phosphatidylglycerol (PG),
39 and Cardiolipin (CL). The effect of the peptides on the structure of 1,2-dipalmitoyl (d62)-sn-
40 glycerol-3-phosphocholine (DPPC)/PE:PG:CL bilayers were also examined by NR. In both model
41 systems, modified clupeine demonstrated a greater effect on the lipid structure. **Charge reduction**
42 **in the modified sample also resulted in improved hydrophobicity, and the formation of thicker**
43 **peptide layers in the membrane models. Some lipid translocation** was observed in the inner tail
44 region ($\sim 69 \pm 0.24\%$ DPPC and $\sim 24 \pm 0.02\%$ PE:PG:CL); and in the outer tail region ($\sim 24 \pm 0.02\%$
45 DPPC and $\sim 56 \pm 0.01\%$ PE:PG:CL). **Improved hydrophobicity and electrostatic interactions with**
46 **lipid head groups, strongly suggests that the modified clupeine may use the carpet mechanisms to**
47 **exert its effect on model membranes. These findings suggest that changing the charge on the native**
48 **peptide changes the way in which the modified peptide disrupts Gram-negative model membranes.**

49

50 **Keywords:** Clupeine, cationic antimicrobial peptide, Gram-negative bacteria, neutron
51 reflectometry, and X-ray reflectometry, and protamine.

52

53

54

55 **1 Introduction**

56

57 Bacteria can have both beneficial and harmful effects in food systems. For example, their
58 use as probiotics (lactic acid bacteria) in fermented foods provide beneficial effects on human
59 health (Ohashi & Ushida, 2009; Doyle, Steenson, & Meng, 2013). On the other hand, approaches
60 to ensure the safety of food components and to combat illnesses caused by food-borne pathogens
61 must confront the global problem of bacterial resistance (Manyi-Loh, Mamphweli, Meyer, &
62 Okoh, 2018). Molecular studies have emphasized that the remarkable ability of bacteria to
63 undermine the efficacy of antimicrobial agents is due in part to their ability to adapt under selective
64 pressure and develop resistance through mutations or by acquiring genes from other bacteria
65 (Canu, A., Malbruny, B., Coquemont, M., Davies, T., Appelbaum, P., & Leclercq, 2002; Spratt,
66 Bowler, Zhang, Zhou, & Smith, 1994). Thus, for the past three decades, a major scientific priority
67 has been the pursuit of new sources of antimicrobial agents with alternate mechanisms of action,
68 which can limit the development of bacterial resistance (Munita & Arias, 2016).

69 In this context, cationic antimicrobial peptides (CAPs) have attracted interest as potential
70 alternatives to conventional antimicrobial agents because they have exhibited broad spectrum
71 inhibitory activity against several foodborne pathogens, and there have only been a few reports of
72 developed resistance (Anaya-López, López-Meza, J., & Ochoa- Zarzosa, 2013). CAPs are found
73 in many organisms including plants and fish (Omardien, Brul, & Zaat, 2016), and some can be
74 cheaply extracted from waste streams (Gill, Singer, & Thompson, 2006). **In spite** of differences in
75 their overall structure and sequence, many CAPs are characterized by their amphipathic domains,
76 and their polycationic nature due to the presence of lysine, arginine or histidine residues (Wu,
77 Maier, Benz, & Hancock, 1999).

78 **Several membrane disruption models including the barrel-stave, carpet, and the toroidal**
79 **pore models have been proposed for CAPs. The validity of these models, and therefore**

80 antimicrobial activity largely depend on the cationic charge and amphipathic nature of CAPs
81 (Straus & Hancock, 2006). In the barrel-stave model (BSM), the amphipathic nature of CAPs is
82 utilized, here their hydrophobic peptide regions align into the lipid environment, whereas the
83 hydrophilic side chains are aligned inward to form trans-membrane pores (Brogden, 2005). It is
84 through these pores that cytoplasmic contents can leak from the cell, and result in cell death.
85 Similarly, in the toroidal pore model, CAPs are inserted into the bilayer and cause the latter to
86 bend and form a pore. As a result, phospholipid head groups and polar peptide surfaces line the
87 pore lumen and local aggregations of varied numbers of peptide molecules within the membrane
88 provide a route of passage of ions (Brogden, 2005). On the other hand, in the carpet model, the
89 peptides bind to the cell surface in an electrostatic manner, and form a layer that alters membrane
90 fluidity and or reduces the barrier properties of the membrane (Pelegriani, del Sarto, Silva, Franco,
91 & Grossi-de-Sa, 2011).

92 Among CAPs, protamine, is a small peptide (4112 Da) which may be extracted from the
93 sperm cells of fish such as herring (clupeine) and salmon (salmine). Similar to most CAPs
94 protamine is very cationic and consists of 31 amino acids, with 20 of those residues being arginine
95 (Suzuki & Ando, 1972). However, unlike most CAPs, protamine is not amphipathic, and lacks
96 secondary structure due to the even distribution of positive charges along the peptide backbone
97 (Bonora, Ferrara, Paolillo, Toniolo, & Trivellone, 1979). Protamine has also exhibited
98 antimicrobial activity toward food-borne pathogenic bacteria but widespread applications in foods
99 are made difficult due to non-specific interactions with food components (Truelstrup Hansen &
100 Gill, 2000; Ueno, Fujita, Yamamoto, & Kozakai, 1988). These non-specific interactions can be
101 overcome by chemically blocking arginine residues with 1,2-cyclohexanedione (CHD), which also
102 reduces the surface charge of the peptide (Potter et al., 2005). The CHD-treated peptide also has

103 improved **antimicrobial activity** as demonstrated by reduced growth of *Listeria monocytogenes* in
104 milk as well as in ground beef (Potter, Truelstrup Hansen, & Gill, 2005) but the effects of the
105 peptides on bacterial membrane structure is not fully known. Accordingly, our objective was to
106 use two complementary biophysical techniques, neutron reflectometry (NR) and X-ray
107 reflectometry (XRR), to investigate the effect of native and modified clupeine on the structure of
108 model monolayer membranes composed of zwitterionic (Phosphatidylethanolamine, PE), and
109 anionic phospholipids (Phosphatidylglycerol, PG and Cardiolipin, CL). These phospholipids are
110 present in the natural, cytoplasmic membrane of Gram-negative bacteria in an approximate 79:17:4
111 mole % ratio (Sohlenkamp & Otto, 2016). The effect of the peptides on the structure of 1,2-
112 dipalmitoyl (d62)-sn-glycero-3-phosphocholine (DPPC)/PE:PG:CL bilayers was also investigated
113 by NR. Understanding the initial steps involved in native and modified clupeine membrane
114 interactions will begin to define characteristics of the peptides and the target bacteria that will be
115 useful in understanding the peptides' mode of action.

116 **2 Materials and Methods**

118 **2.1 Materials**

119
120 DPPE, 1,2-dipalmitoyl-glycero-3-phosphoethanolamine, MW 691.97 (zwitterionic and
121 synthetic purity > 99%); DPPG, 1,2-dipalmitoyl-sn-glycero-3-[phosphor-rac-1-glycerol] (anionic
122 sodium salt), MW 744.96; and 1,1',2,2'-tetramyristoyl cardiolipin (anionic sodium salt), MW
123 1,285.62 were all purchased from Avanti Polar Lipids (Alabaster, AL, USA). Stock solutions of
124 all lipids were prepared using a 3:1 mixture of HPLC grade chloroform to methanol (Sigma-
125 Aldrich, Oakville, ON, Canada) in a ratio (PE:PG:CL; 79:17:4 mole %), **hereafter referred to as**
126 **PPC** and stored at -20°C.. Native clupeine (clupeine sulfate (MW 4112 Da, P4505)), L-arginine,
127 0.1 M HCL solution, CHD (MW 112.13 g/mol), 8-hydroxyquinoline, sodium hydroxide, liquid

128 bromine, and HPLC grade chloroform were obtained from Sigma-Aldrich (Oakville, Oakville,
129 ON, Canada):

130 **2.2 Clupeine Modification**

131
132 To reduce the surface charge of arginine CHD (2.8 g) was dissolved in 500 mL of 0.2 M
133 boric acid buffer (pH 8.5) then 2.5 g of native clupeine was added and the contents of each flask
134 stirred for 20 s (Potter et al., 2005). The samples were incubated at 37°C for 2.5 min and then 500
135 mL of cold 5 % (v/v) acetic acid was added. Control samples were prepared in a similar manner
136 except that no CHD was added to the reaction flasks. The modified samples were concentrated to
137 200 mL, and then exhaustively dialyzed in a Prep/Scale Millipore Model P34404 ultrafiltration
138 apparatus (Millipore, Toronto, ON, Canada) equipped with 900 cm², 1000 Da tetrafluoroethylene
139 (TFE) filters and flushed with five volumes of 1% (v/v) acetic acid and ten volumes of distilled,
140 deionized water (DDW) and concentrated once again to 200 mL as described by Potter et al.
141 (2005). Finally, the purified samples were frozen at -30°C and then freeze dried (Labconco,
142 Missouri, USA). Stock solutions were prepared by dissolving 0.1 g of the powder in 40 mL of 1%
143 (v/v) acetic acid. Working solutions were prepared by diluting the stock solutions 1:50 with DDW.
144 The Sakaguchi reaction (Sakaguchi, 1950; Potter et al., 2005), which is specific for arginine, was
145 used to determine the unmodified arginine residues in the CHD-treated clupeine. The percent
146 modification of arginine residues was determined using an arginine-HCl standard curve and taking
147 into account that ~20 of the 30 amino acid residues in clupeine are arginine (Ando et al., 1973).
148 Only CHD-treated clupeine with 10% of the arginine residues modified was chosen for further
149 testing because it has been reported that moderate reductions in charge led to improved
150 antimicrobial efficacy (Potter et al., 2005).

151 **2.3 Peptide Surface Hydrophobicity**

152

153 The surface hydrophobicity (S_o) of the native and modified samples was measured using
154 a fluorescent probe, 6-propionyl-2-(N,N-dimethylamino) naphthalene (PRODAN) as outlined by
155 Alizadeh-Pasdar and Li-Chan (2000) with modifications. A PRODAN standard curve was
156 developed using concentrations ranging from 0 to 0.95 μ M. Using this PRODAN binding curve,
157 it was possible to measure the amount of PRODAN bound to the peptide samples. PRODAN (20
158 μ L, 7.6 mM) was added to 4 mL of peptide in a 0.01 M phosphate buffer (pH 7). After 15 min
159 incubation in the dark, the relative fluorescent intensity (RFI) was measured using a Photo
160 Technology International (PTI) fluorescence spectrophotometer, with excitation and emission
161 wavelengths set at 390 and 470 nm, respectively.

162 **2.4 Zeta Potential**

163 The net charge density of the peptides was measured as zeta potential (mV) using a Zetasizer
164 Nano Model ZS (Malvern Instruments, Derbyshire, UK) as outline by Paulson and Tung (1987)
165 with modifications. Measurements were made at 20°C in triplicate. The zeta potential was
166 calculated from the electrophoretic mobility of individual particles, measured using laser Doppler
167 velocimetry (Malvern Instruments Ltd, 2004).

168 **2.5 Surface Pressure Measurements**

169
170 Surface pressure measurements on a Langmuir trough (model 611 Nima Technology,
171 Coventry, England) interfaced with a computer data acquisition system were carried out by the
172 Wilhelmy plate method as described by Lad, Birembaut, Clifton, Frazier, Webster, & Green,
173 (2007). Clean troughs were filled with 80 mL of 0.02 M phosphate buffer (pH 7), and 20 μ L of
174 the lipid solution in chloroform was spread dropwise using a Hamilton syringe (Hamilton
175 Company, Reno, NV) on the surface of the buffer to form a monolayer. The lipid monolayer was
176 compressed to a target surface pressure of ~ 25 mN m^{-1} . Control checks were carried out for ~ 4.2

177 h on the bare **PPC** monolayers to determine their stability. For each experiment, the compressed
178 film was relaxed for 20 min at $\sim 25 \text{ mN m}^{-1}$ prior to the addition of 1 mL of native or modified
179 clupeine solution to the subphase (final peptide concentration of $0.48 \mu\text{M}$). Compression isotherms
180 were recorded as surface pressure (π) vs. area (A) curves prior to the addition of the peptides and
181 on addition of the peptide to the subphase, and plots of surface pressure vs. time were recorded to
182 follow adsorption of the peptides to the lipid layer. All compressions were repeated until a
183 reproducible trace was obtained and the final surface pressure values had a standard deviation of
184 $\pm 1 \text{ mN m}^{-1}$. Similar experiments were carried out using the negatively charged phospholipid,
185 DPPG, as a control.

186 **2.6 Neutron Reflectometry Measurements on **PPC****

187
188 NR measurements were carried out using the white beam SURF reflectometer at the
189 Rutherford Appleton Laboratory (Didcot, Oxfordshire, UK), using neutron wavelengths from 0.5
190 to 6.5 \AA . The beam intensity was calibrated with respect to a clean D_2O surface. The sample
191 preparation and NR method were carried out as described by Clifton, Sanders, Hughes, Neylon,
192 Frazier, & Green (2011) with some modifications. Briefly, all the NR experiments were performed
193 at room temperature and the lipid films were prepared by spreading the **PPC** lipid mix (from the
194 stock solution) in a $200 \times 400 \text{ mm}$ Langmuir trough (Nima Technology, Coventry, UK) containing
195 a 20 mM phosphate buffer (pH 7.0). Films were compressed to a surface pressure of 23 mN m^{-1}
196 and the films were relaxed for 20 min at 23 mN m^{-1} prior to the addition of native or CHD-treated
197 clupeine solutions ($0.48 \mu\text{M}$) to the lipid monolayer. NR curves were recorded at two angles of
198 incidence ($\theta = 1.5$ and 0.8°) to yield a momentum transfer range of $\sim 0.01 - 0.6 \text{ \AA}^{-1}$ both before and
199 after the addition of native or CHD-treated clupeine. NR was measured under multiple isotopic
200 contrasts and this was achieved by using hydrogenated and deuterated lipids in a **non-reflecting**

201 water subphase compared to air, NRW (8% D₂O, 92% H₂O), and D₂O. Measurements using
202 hydrogenated lipids (h-lipids) on NRW were done to observe protein binding since the h-lipid will
203 be largely non-reflecting ($\rho(h - lipid) = -0.39 \times 10^{-6} \text{ \AA}^{-2}$), where ρ represents the scattering
204 length density (SLD). Repeat experiments using isotopic contrasts with d-lipid ($\rho(d - lipid) =$
205 $7.5 \times 10^{-6} \text{ \AA}^{-2}$) on NRW were also done to reveal any changes in lipid layer structure caused by
206 the interaction. Contrasts of h-lipid on D₂O were also done to enable differentiation between
207 peptide adsorbed beneath the interface and the lipid head group (Clifton, Neylon, & Lakey 2013a).

208 **2.7 X-Ray Reflectometry Measurements on PPC**

209 X-ray reflectometry experiments were performed at the I07 beamline at the Diamond Light
210 Source (Harwell Science and Innovation Campus, Didcot, Oxfordshire, UK). The sample
211 preparation and method described by Clifton et al. (2012) was carried out. Experiments were
212 performed at room temperature and the lipid films were prepared by spreading the PPC lipid mix
213 (from the stock solution) in a 200 x 400 mm Langmuir trough containing a 20 mM phosphate
214 buffer (pH 7.0). The films were compressed to a surface pressure of 23 mN m⁻¹ and then relaxed
215 for 20 min at 23 mN m⁻¹ prior to the addition of native or CHD-treated clupeine solutions (0.48
216 μM). A monochromatic X-ray wavelength of 0.992 \AA (corresponding to a photon energy, E of
217 12.5keV) was used and a fast shutter was applied to avoid over-exposure to the X-ray beam.

219 The experiments were also performed in a helium atmosphere, the reflectivity profiles were
220 measured in a Q_z range of 0.01 to 0.8 \AA^{-1} and data were collected on a Dectris Pilatus 100 k
221 detector. XRR data were reduced by performing a normalisation and a “footprint correction” step.
222 There were three parts to the normalisation, the first part involved dividing by the incident flux
223 since this varies with the incident angle. The second part involved stitching the three regions
224 together; by overlapping points at the extremes of each region. The third part involved scaling the

225 data so that reflectivity at the critical edge was equal to one. The detector also used two ‘regions
226 of interest’ (ROI) to simultaneously measure the signal, and this background was subtracted from
227 all the data sets (Clifton et al., 2012).

228 **2.8 Bilayer Deposition and Neutron Reflectometry Measurements**

229
230 Gram-negative model, single bilayer membranes were prepared at the ISIS Biological
231 Sample Laboratory (Rutherford, England) as outlined by Clifton et al. (2013b). NR measurements
232 were carried out using the white beam SURF reflectometer, using neutron wavelengths from 0.5
233 to 6.5 Å. The collimated neutron beam was reflected from the silicon-liquid interface at three
234 different glancing angles of incidence, 0.35°, 0.65° and 1.5°.

235 A neutron flow-cell was placed at the bottom of a clean Langmuir-Blodgett (LB) trough
236 (KSV-Nima, Biolin Scientific, Finland) and the cell was flushed with ultrapure water (Millipore,
237 18.2 MΩ cm⁻¹) to remove air bubbles and was then filled with 20 mM phosphate buffer (pH 7.0)
238 A Piranha-cleaned (H₂O₂/H₂SO₄/H₂O 1:4:1) silicon (SiO₂) crystal was then mounted onto the
239 dipping mechanism of the trough in a vertical position and with the active face away from the
240 center, then the block was submerged under the buffer. Two bilayers were prepared and 150 μL
241 of tail-hydrogenated or deuterated 1,2-dipalmitoylphosphatidylcholine (h-DPPC and d-DPPC) in
242 1 mg/mL in chloroform, was spread onto the clean water surface. The lipid was compressed to an
243 initial pressure of 10 mN m⁻¹ and then equilibrated for 15 min. The lipid layer was then compressed
244 to 35 mN m⁻¹ at a rate of 3 mm min⁻¹. Pressure-area isotherms were recorded to confirm the
245 homogeneity of the film.

246 For LB deposition of the inner bilayer leaflet, the submerged silicon crystal was lifted
247 through the air-water interface at a rate of 3 mm/min and at a constant pressure of 35 mN m⁻¹. The
248 entire LB deposition procedure took 45 min. For Langmuir Schaefer (LS) transfer, a clean neutron

249 flow-cell was placed in the bottom of the trough before it was filled with cold 20 mM Hepes buffer
250 (pH 7.2). A monolayer was formed on the surface by adding 150 μL of the PE:PG:CL (79:17:4
251 mole %) lipid mix, and the latter was compressed to 35 mN m^{-1} . The silicon crystal containing the
252 LB-deposited DPPC monolayer was placed on the dipping mechanism of the trough, with the
253 crystal face parallel to the water surface. The silicon crystal with the deposited LB film was then
254 dipped through the interface at a constant rate of 3 mm min^{-1} and lowered into the neutron flow-
255 cell at the bottom of the trough. Native or CHD-treated clupeine (0.48 μM) were added to the cell
256 in a 20 mM Hepes buffer (pH 7).

257 **2.9 Reflectivity Data Analysis for Monolayers**

258 NR and XRR data were analyzed using a Matlab version of RasCal (version 1.1.2, Hughes,
259 A., ISIS Spallation Neutron Source, Rutherford, Appleton Laboratory). In RasCal, structures
260 across the interface were modeled as a series of layers and each layer was described by three main
261 parameters: thickness (τ), SLD (ρ), and roughness (Clifton et al., 2013a). The SLD of the lipids
262 (head groups and tails), solvents and peptides were calculated using equation 1:
263

264 Eq. 1

$$265 \quad \rho = \frac{\sum b}{V}$$

266 Where b represented the SL for each element and V represented the molecular volume (Lad, 2006).
267 The XRR and NR data were first fitted individually then fitted simultaneously as described by
268 Nelson (2006) and Clifton et al. (2012) to place restrictions on the NR fit. The thickness and
269 roughness parameters were linked in a single model and the SLD and background values were
270 allowed to vary (Nelson, 2006).

271 Bare lipid monolayers with no peptides were divided into two layers, the first, a lipid chain
272 layer containing CH_3 and CH_2 groups and the second, a head group layer containing the lipid head

273 groups (Dabkowska, Fragneto, Hughes, Quinn, & Lawrence, 2009). This classification was based
274 on two assumptions: (1) the first layer contained only lipid component and the second layer
275 contained only the head group; (2) the second assumption was related to the area per molecule and
276 assumed that this value was the same for both the lipid head group and the tail region (Clifton et
277 al., 2011). However, in order to measure peptide binding to the monolayer, a third layer was
278 included in the model to represent the presence of the peptides below the lipid monolayer
279 (Saunders, Clifton, Frazier, & Green, 2016). A set of reflectivity profiles measured under the three
280 isotopic contrasts hydrogenated (h)-lipid in NRW; h-lipid in D₂O and deuterated (d)-lipid in NRW
281 were fitted together and the large difference between the scattering lengths of hydrogen (-0.56 x
282 10⁻⁶ Å⁻²) and deuterium (6.35 x 10⁻⁶ Å⁻²) was used to detect the location of different components
283 in the monolayer. The parameters of the measured data were then fitted to the theoretical model
284 until the best fit was achieved. The quality of the fit was also assessed visually. The fitted SLD for
285 each isotopic contrast was related to the volume fraction of each component using equation 2,
286 where Φ represented the volume fraction, ρ represented the SLD, $\rho_{(D)}$ and $\rho_{(H)}$ represented the
287 fitted SLD and $\rho_{(D-L)} - \rho_{(H-L)}$ represented the calculated SLD.

288 Eq. 2

$$\Phi (lipid) = \frac{\rho(D) - \rho(H)}{\rho(D - L) - \rho(H - L)}$$

290 The SLDs and the molecular volume for the native and CHD-treated peptides were calculated as
291 outlined in the ISIS Biomolecular SLD Calculator (<http://psldc.isis.rl.ac.uk/Psldc/>). To calculate
292 the SLD for the lipid mixture of PPC, the SLD of each individual lipid head and tail was calculated
293 and then multiplied by its fraction in the mixture. The molecular volumes of the lipid components
294 were calculated using the Molinspiration Property Calculator
295 (<http://www.molinspiration.com/cgi-bin/properties>). The area per molecule (A) occupied by the

296 peptide and the lipid in each layer and the surface excess (Γ) for each component in the system
297 were calculated using equations 3 and 4, where b represented the scattering length, ρ represents
298 the SLD, and τ represented the layer thickness obtained from the model fit (Clifton et al., 2011).

299

$$300 \quad A = \frac{\sum b}{\tau \phi \rho} \quad \text{Eq. 3}$$

301

$$302 \quad \Gamma = \frac{MW}{A * 6.02 \text{ g/mol}} \quad \text{Eq. 4}$$

303

304 **2.10 Reflectivity Data Analysis for Bilayers**

305

306 Model biomembranes systems composed of either tail deuterated or tail hydrogenated
307 DPPC as the inner leaflet and hydrogenated-PPC as the outer leaflet were prepared, then NR
308 experiments were carried out using three different solution subphases; (1) D₂O (100%, $\rho=6.35 \times$
309 10^{-6} \AA^{-2}); (2) silicon matched water (SMW, 38% D₂O and 62% H₂O, $\rho=2.07 \times 10^{-6} \text{ \AA}^{-2}$); and (3)
310 100% water ($\rho=-0.56 \times 10^{-6} \text{ \AA}^{-2}$). Each deuterated and hydrogenated lipid bilayer was measured
311 under all three isotopic contrasts (D₂O; SMW and H₂O) thus resulting in a total of six different
312 reflectivity profiles. The large difference between the SLD for deuterated-DPPC ($7.45 \times 10^{-6} \text{ \AA}^{-2}$)
313 and hydrogenated-DPPC ($-0.39 \times 10^{-6} \text{ \AA}^{-2}$) tail regions made it possible to determine structural
314 parameters from the tail region within each individual bilayer. Reflectivity data were obtained for
315 the six contrasts before and after the addition of native and CHD-treated clupeine and the data
316 were analyzed as described in Clifton et al. (2013) using a Matlab version of RasCal. The three
317 membrane components in the bilayer were DPPC, PPC and water and their individual
318 contributions to the bilayer were determined from the fitted values obtained for the tail deuterated-

319 DPPC SLDs in the three subphase mixtures (100% D₂O, SMW (30% D₂O and 100% water). The
 320 SLD (ρ) of a given layer was related to the three membrane components by the following equation:

$$321 \quad \rho = (\rho_{DPPC})(\phi_{DPPC}) + (\rho_{PPC})(\phi_{PE:PG:CL}) + (\rho_{Water})(\phi_{Water}) \quad \text{Eq. 2}$$

322
 323
 324 Where ρ represented the SLD of a given layer and ρ_{DPPC} , ρ_{PPC} and ρ_{Water} represented the SLD
 325 of DPPC, PPC and water respectively, while ϕ_{DPPC} , ϕ_{PPC} and ϕ_{Water} represented the volume
 326 fractions of the same components. Because the DPPC and PPC lipid tail regions do not contain
 327 labile hydrogens and would not undergo solvent-contrast-related changes in SLD (Clifton et al.,
 328 2013b), the volume fraction of water was determined from the following equation:

$$329 \quad \phi_{Water} = \frac{\rho_{water\ contrast1} - \rho_{water\ contrast2}}{\rho_{water1} - \rho_{water2}} \quad \text{Eq. 6}$$

330
 331 Where $\rho_{water\ contrast1}$ and $\rho_{water\ contrast2}$ represented the SLDs of the same layer in any two of
 332 the three contrasts (H₂O, SMW or D₂O) used, while $\rho_{water1} - \rho_{water2}$ represented the SLDs of
 333 each solvent mixture. Once the volume fraction of water (ϕ_{Water}) was determined, then the DPPC
 334 fraction in the d-DPPC/h-PPC bilayer system was determined using equation 6.
 335

$$336 \quad \rho - (\rho_{water}\phi_{water}) = (\rho_{DPPC\ tails})(\phi_{DPPC\ tails}) + (\rho_{PPC\ tails})(\phi_{PPC\ tails}) \quad \text{Eq. 7}$$

337
 338 Equation 7 was used to find the value of $\rho - (\rho_{water}\phi_{water})$, which was needed in order to fully
 339 complete equation 8:
 340

$$341 \quad \phi_{DPPC\ tails} = \left(\frac{(\rho - (\rho_{(water)}\phi_{water}) - (\rho_{PPC\ tails}(1 - \phi_{water})))}{(\rho_{d-DPPC\ tails} - \rho_{PPC\ tails})} \right) \quad \text{Eq. 8}$$

342
 343

344 Once the relative contribution of the $\phi_{DPPC\ tails}$ were determined, then the relative contributions
345 of the PPC tails to the bilayer were determined by using equation 9:

346
347
$$\phi_{PPC} = 1 - (\phi_{DPPC\ tails} + \phi_{water})$$
 Eq. 9
348

349 **2.11 Model to Experimental Data Fitting Analyses**

350
351 The ‘bootstrap’ error analysis function in RasCal was used to obtain model to experimental data
352 fitting errors as previously described by (Clifton et al., 2012; Clifton et al., 2013b). The original
353 data set was resampled, then new data sets were fitted using the methods described earlier. “The
354 parameter value distributions obtained across these fits were used to estimate errors, and these
355 values were then propagated through the calculations of the derived parameters according to
356 error treatment methods” (Clifton et al., 2013b).

357 **3 Results and Discussion**

358 **3.1 Net charge density and surface hydrophobicity**

359
360 The native peptide was far less hydrophobic than the modified sample (P=0.02, n=3) at the
361 pH level tested (Figure 1A). Since the native clupeine is highly cationic in nature, the use of an
362 anionic probe such as 1-anilinonaphthalene-8-sulfonic acid (ANS) would have resulted in greater
363 interaction with the positively charged sites on the peptide, thus overestimating the
364 hydrophobicity. This supports the use of the uncharged probe PRODAN which eliminated the
365 possible electrostatic contributions in the hydrophobicity measurements (Alizadeh-Pasdar & Li-
366 Chan, 2000). The measured zeta potential of the native clupeine was 7.2 ± 0.2 mV, which was
367 similar to the value reported by Arbab et al. (2004). Conversely, the modified sample registered a
368 zeta potential of 5.3 ± 0.1 mV.
369

370 **3.2 Peptide binding to lipid monolayer using surface pressure measurements**

371

372 The surface pressure change on addition of clupeine to a compressed **PPC** monolayer at
373 the air/water interface was investigated as a function of time (Figure 1). The data showed an
374 increase in surface pressure for CHD-treated clupeine that was not seen for the native peptide. The
375 maximum increase seen after 300 min from addition of the treated clupeine to the subphase was
376 approximately 11 mN/m. This suggests that the CHD-treated clupeine had penetrated into the lipid
377 layer leading to increase compression of the layer, an effect previously reported by (Abuillan et
378 al., 2013; Oliveira et al., 2009). For the native clupeine no increase in surface pressure was
379 observed, although a gradual decrease was seen that could be due to lipid removal at the surface,
380 but was more likely a consequence of the stability of the lipid layer and not an indication of any
381 clupeine interaction. Importantly, this could have been resolved if an equivalent volume of peptide-
382 free buffer was added to the subphase and the same decrease in surface pressure was observed.
383 Conversely, if no effect on surface pressure was observed over the same time period, this would
384 suggest that the peptide did not sit at the air-water surface (Dabkowska et al., 2009).

385 **3.3 Impact of peptide on lipid monolayer structure**

386 NR and XRR reflectivity data were fitted simultaneously to provide characterisation of the
387 interfacial layer structure before and after peptide addition. The **PPC** monolayer characterization
388 prior to peptide addition was determined using two reflectivity profiles, the d-**PPC** on an NRW
389 buffer subphase (NR) and the h-**PPC** on a H₂O phosphate buffer subphase (XRR). **Models of the**
390 **XRR fits are not shown.** A two layer model was used to fit the data, where layer 1 was the acyl
391 chain region with a thickness (τ) of 15 ± 0.64 Å and a volume fraction (Φ_L) of 0.97 ± 0.02 , whereas
392 layer 2 was the lipid head group of the condensed PE:PG:CL monolayer, with a τ of 12.9 ± 1.2 Å
393 (Table A2). Ciumatic et al. (2017) and Dabkowska et al. (2009) have also reported similarly thin
394

395 hydrophobic chain regions for DPPC or DPPG and for 1,2-dioleoyl-sn-glycero-3-phosphocholine
396 or palmitoyl-oleoyl-glycero-3-phosphoserine (DOPC/ POPS) monolayers.

397 A third layer was included into the model to allow for fitting of clupeine adsorbed below the
398 lipid layer (Figure 2). In addition, the hydrogenated contrasts in NRW proved to be informative in
399 identifying the contribution of the peptide to the monolayer. As shown in Figure 2 A, the three
400 layer model proposed for native clupeine adsorbed to the condensed phase PPC monolayer, fitted
401 the data well. Peptide binding in the presence of native clupeine showed minimal adsorption in the
402 lipid layer (surface excess (Γ) = 0.005 ± 0.02), but a greater effect was observed in the lipid head
403 group region (Γ = 0.297 ± 0.02) and a thickening of the peptide layer (τ , increased from $15.0 \pm$
404 0.01 \AA to $15.3 \pm 0.07 \text{ \AA}$). Conversely, in the presence of the modified peptide a greater effect on
405 the structure of the monolayer was observed (Figure 3). For example, there was a 25% and 15%
406 increase in surface excess and a peptide layer thickness, respectively, compared to the measured
407 values in the presence of the native peptide (Table 1). Slight increases in SLD, $1.07 \pm 0.06 \times 10^{-6}$
408 \AA^{-2} or $1.69 \pm 0.05 \times 10^{-6} \text{\AA}^{-2}$ in the presence of native or CHD-treated clupeine, respectively, were
409 also observed (Table 1). Notable, the difference in the fitted SLDs and the total adsorbed peptide
410 was almost two-fold in the presence of the modified peptide compared to the native peptide.

411 The requirement of a third layer below the monolayer supports the observation from the
412 surface pressure studies for the modified clupeine, and confirms that the peptide interacted with
413 the PE:PG:CL monolayer (Figure 1). More importantly, the advantage of using two different
414 techniques to characterize peptide interaction with the PPC monolayer is emphasized since, NR is
415 sensitive to the total amount of material at the interface. Thus although the presence of native
416 clupeine on the PPC monolayer led to a decrease in surface pressure change, NR measurements
417 clearly revealed a thickening of the layer (Table1). Work with Puroindoline-b (pin-b) protein

418 mutants has also shown little change in surface pressure when the proteins were inserted onto
419 DPPC or DPPG monolayers, however, similar to native and CHD-treated clupeine, NR revealed
420 most of the peptide situated below the lipid region (Clifton, Lad, Green, & Frazier, 2007; Clifton,
421 Green, Hughes, & Frazier, 2008). Moreover, NR and XRR methods were advantageous since
422 differences in the radiation source (XRR versus NR) result in different scattering length densities
423 (SLD), and selective SLD modification with deuterium (D₂O) labeling made it possible to reveal
424 subtle changes in membrane structure in the presence of the peptides (Lopez-Rubioa, & Gilbert,
425 2009).

426 **3.4 Impact of Peptides on Bilayer Structure**

427
428 To validate that the trends observed with the monolayer work were not dependent on the
429 lipid layer model used, bilayer studies were performed. Figure 4 shows the NR profiles and data
430 fits of bilayers in the presence of native (4A), and modified clupeine (4B) examined under three-
431 solution contrasts (D₂O, SMW and H₂O). In the outer lipid head group region there was a change
432 in SLD from 2.5 to 2.2 or 2.3 x 10⁻⁶Å⁻² in the presence of native or modified clupeine, respectively
433 (Table 2). The decrease in SLD may be explained by lipid removal from the bilayer in the presence
434 of the peptides. Lipid loss was also accompanied by an increase in hydration of the lipid head
435 group, from 17.9 ± 12.7% on the bare bilayer compared to 26.9 ± 5.5% in the presence of native
436 clupeine and 48.2 ± 11.5% in the presence of the modified clupeine. The greater degree of
437 hydration in the lipid head group region in the presence of modified peptide compared to the native
438 peptide is observed as a broader peak in Figure 4 D compared to Figure 4 F and may also indicate
439 greater solvent penetration.

440 The model used to fit the reflectivity data from the deuterated lipids (Figure 4B) showed
441 that it was possible to form asymmetric bilayers with ~90% DPPC inner leaflet composition and

442 an outer layer of ~80% PPC. Although it is now known how closely the model membrane fits the
443 real membrane, similar percent coverages have been reported by Fernandez et al. (2013). Lipid
444 translocation was also observed in the inner tail region ($\sim 69 \pm 0.24\%$ DPPC and $\sim 24 \pm 0.02\%$ PPC)
445 and in the outer tail region ($\sim 24 \pm 0.02\%$ DPPC and $\sim 56 \pm 0.01\%$ PPC) (Table 2). Lipid
446 translocation may have resulted due to lateral heterogeneity in the bilayer which leads to the
447 formation of domains (Epanand, 2013). Vorobyov and Allen (2011) discussed the importance of
448 bilayer charge in mediating peptide interaction and showed that adsorption of cationic peptides to
449 anionic bilayers is significantly higher than in zwitterionic membranes. Importantly, electrostatic
450 interactions between peptides and anionic lipids has also been postulated as another factor that
451 supports the formation of domains (Epanand, 2013). In the present study it is possible that the
452 peptides could exert part of their effect by changing lateral organization in the membrane.
453 Increased hydrophobicity of the modified clupeine may also explain the increased magnitude of
454 the effect on the lipid structure. Furthermore, thicker peptide layers in the presence of the modified
455 peptide ($11.04 \pm 6.0 \text{ \AA}$ versus $4.15 \pm 2.9 \text{ \AA}$ in the presence of the native peptide) (Table 2), implies
456 the accumulation of peptides to form a layer that can interact with negatively charged components
457 in the membrane. Thus, it appears that both hydrophobic and electrostatic interactions may govern
458 the mode of action of the modified clupeine, and strongly suggests that the modified clupeine may
459 use the carpet mechanisms to exert its effect on model membranes. These observations support the
460 findings of Pink, Hasan, Quinn, Winterhalter, Mohan, and Gill (2014) who reported that native
461 clupeine can internalize and kill some Gram-negative bacteria without lysis or pore formation.

462 **Conclusion**

463 The initial interactions of native and CHD-treated clupeine in model membranes has been
464 investigated by combining NR and XRR techniques. In the less complex monolayer system,

465 quantitative amounts of peptides could be determined as surface excess values in the presence of
466 both peptides. Lipid translocation was observed in the inner acyl chains of the bilayer membrane
467 however, but the peptides were not able to penetrate the bilayer membrane. Similar effects on the
468 model membrane structure were observed, although peptide perturbation of the membranes
469 appeared different. Increased hydrophobicity along with electrostatic interactions of the modified
470 peptide were attributed to the improved peptide-lipid interactions. A more comprehensive
471 understanding of the safety and toxicology of these peptide is required before they can be
472 considered for food applications in Canada.

473 **Acknowledgments**

474 The authors acknowledge support from the Natural Sciences and Engineering Research Council
475 of Canada and a direct access beamtime award. We thank Dr. Michael Sanders for assistance
476 with the surface pressure experiments, and Dr. Filip Ciesielski and Dr. Arwel Hughes for
477 technical assistance during the bilayer experiments.

478 **Author Contributions**

479 M. English analysed the data and drafted the manuscript. L. Clifton and O. Florek contributed to
480 the acquisition of NR data and the interpretation of the results. T. Arnold assisted with the
481 collection of the X-ray data. A. Paulson, R. Green and R. Frazier contributed to critically
482 revising the manuscript and giving final approval of the version to be submitted.

483

484

485

486

487

489 **References**

- 490 Abuillan, W., Schneck, E., Korner, A., Brandenburg, K., Gutschmann, T., Gill, T., Vorobiev, A.,
491 Konovalov, O., & Tanaka, M. (2013). Physical interactions of fish protamine and
492 antiseptic peptide drugs with bacterial membranes revealed by combination of specular
493 x-ray reflectivity and grazing-incidence x-ray fluorescence. *Physical Review*, 88, 1-11.
494 doi:10.1103/PhysRevE.88.012705
- 495
- 496 Alizadeh-Pasdar, N., & Li-Chan, E. (2000). Comparison of protein surface hydrophobicity
497 measured at various pH values using three different fluorescent probes. *Journal of*
498 *Agricultural Food Chemistry*, 48, 328–334. doi: 10.1021/jf990393p
- 499
- 500 Anaya-López, J., López-Meza, J., and Ochoa-Zarzosa, A. (2013) Bacterial resistance to cationic
501 antimicrobial peptides. *Critical Reviews in Microbiology*, 39, 180-195.
502 doi: 10.3109/1040841X.2012.699025
- 503
- 504 Arbab, A., Yocum, G., Kalish, H., Jordan, E., Anderson, S., Khakoo, A., Read, E., & Frank, J.
505 (2004). Efficient magnetic cell labeling with protamine sulfate complexed to ferumoxides
506 for cellular. *MRI. Blood*, 104, 1217-1223. <https://doi.org/10.1182/blood-2004-02-0655>.
- 507
- 508 Bonora, G., Ferrara, L., Paolillo, L., Toniolo, C., & Trivellone E. (1979). ¹³C Nuclear magnetic
509 resonance of protamines. The three main components of clupeine. *European Journal of*
510 *Biochemistry*, 93: 13–21.
- 511
- 512 Boyle, C., Hansen, L., Hinnenkamp, C., & Ismail, B. (2018). Emerging Camelina protein:
513 extraction, modification, and structural/functional characterization. *Journal of the*
514 *American Oil Chemists Society*, 95, 1049–1062. doi: 10.1002/aocs.12045
- 515
- 516 Broniatowski, M., Mastalerz, P., & Flasiński, M. (2015). Studies of the interactions of ursane-
517 type bioactive terpenes with the model of Escherichia coli inner membrane -Langmuir
518 monolayer approach. *Biochimica et Biophysica Acta*, 1848, 469–476.
519 doi.org/10.1016/j.bbamem.2014.10.024
- 520
- 521 Canu, A., Malbruny, B., Coquemont, M., Davies, T., Appelbaum, P., & Leclercq, R. (2002).
522 Diversity of ribosomal mutations conferring resistance to Macrolides, Clindamycin,
523 Streptogramin, and Telithromycin in *Streptococcus pneumoniae*. *Antimicrobial Agents*
524 *and Chemotherapy*, 46, 125-131. doi: 10.1128/AAC.46.1.125-131.2002
- 525
- 526 Ciumac, D., Campbell, R., Xu, H., Clifton, L., Hughes, A., Webster, J., Lu, J. (2017).
527 Implications of lipid monolayer charge characteristics on their selective interactions with
528 a short antimicrobial peptide. *Colloids and Surfaces B: Biointerfaces*, 150, 308–316.
529 doi.org/10.1016/j.colsurfb.2016.10.043
- 530

531 Clifton, L., Ciesielski, F., Skoda, M., Paracini, N., Holt, S., & Lakey, J. (2016). The effect of
532 lipopolysaccharide core oligosaccharide size on the electrostatic binding of antimicrobial
533 proteins to models of the Gram-negative bacterial outer membrane. *Langmuir*, 32, 3485–
534 3494. doi: 10.1021/acs.langmuir.6b00240
535

536 Clifton, L., Skoda, M., Le Brun, A., Ciesielski, F., Kuzmenko, I., Holt, S., & Lakey, J. (2015).
537 Effect of divalent cation removal on the structure of gram-negative bacterial outer
538 membrane models. *Langmuir*, 31, 404–412. doi: 10.1021/la504407v
539

540 Clifton, L., Neylon, C., & Lakey, J. (2013a). Examining protein-lipid complexes using neutron
541 scattering. *Methods in Molecular Biology*, 974, 119-150. doi: 10.1007/978-1-62703-275-
542 9_7
543

544 Clifton, L., Skoda, M., Daulton, E., Hughes, A., Le Brun, A., Lakey, J., & Holt, S. (2013b)
545 Asymmetric phospholipid: lipopolysaccharide bilayers; a Gram-negative bacterial outer
546 membrane mimic. *Journal of the Royal Society Interface*, 10, 1-11.
547 doi:10.1098/rsif.2013.0810
548

549 Clifton, L., Sanders, M., Hughes, A., Neylon, C., Frazier, R., and Green, R. (2011). Lipid
550 binding interactions of antimicrobial plant seed defence proteins: puroindoline- α and β -
551 purothionin. *Physical Chemistry Chemical Physics*, 13, 17153–17162. doi:
552 10.1039/c1cp21799b
553

554 Clifton, L. A., Green, R. J., Hughes, A. V., & Frazier, R. A. (2008). Interfacial structure of wild-
555 type and mutant forms of Puroindoline-b bound to DPPG monolayers. *The Journal of*
556 *Physical Chemistry B*, 112, 15907–15913.
557

558 Clifton, L. A., Lad, M. D., Green, R., J., & Frazier, R. A. (2007). Single amino acid substitutions
559 in Puroindoline-b mutants influence lipid binding properties. *Biochemistry*, 46, 2260-
560 2266.
561

562 Dabkowska, A., Fragneto, G., Hughes, A., Quinn, P., & Lawrence, M. (2009). Specular neutron
563 reflectivity studies of the interaction of Cytochrome c with supported
564 phosphatidylcholine bilayers doped with phosphatidylserine. *Langmuir*, 25, 4203-4210.
565 doi: 10.1021/la802926k
566

567 Del Nobile, M., Conte, A., Cannarsi, M., & Sinigaglia, M. (2009). Strategies for prolonging the
568 shelf life of minced beef patties. *Journal of Food Safety*, 29, 14–25. doi: 10.1111/j.1745-
569 4565.2008.00145.x
570

571 Doyle, M., Steenson, L., & Meng, J. (2013). Bacteria in food and beverage production. In:
572 Prokaryotes, applied bacteriology and biotechnology. Rosenberg, E., DeLong, E., Lory,
573 S., Stackebrandt, E., and Thompson, F. (Ed.), 241- 256. Springer Berlin Heidelberg.
574

575 Epanand R.M. (2013) Lipid Domains. In: Roberts G.C.K. (Eds) Encyclopedia of Biophysics.
576 Springer, Berlin, Heidelberg. <https://doi.org/10.1007/978-3-642-16712-6>

577
578 Fernandez, D., Le Brun, A., Whitwell, T., Sani, M., James, M., & Separovic, F. (2012). The
579 antimicrobial peptide aurein 1.2 disrupts model membranes via the carpet mechanism.
580 *Physical Chemistry Chemical Physics*, 14, 15739–15751.
581 doi: 10.1039/c2cp43099a
582
583 Gerelli, Y., Porcar, L., and Fragneto, G. (2012). Lipid rearrangement in DSPC/DMPC bilayers: a
584 neutron reflectometry study. *Langmuir*, 28, 15922–15928. doi: 10.1021/la303662e
585
586 Gill, T., Singer, D., & Thompson, J. (2006). Purification and analysis of protamine. *Process*
Biochemistry, 41, 1875–1882. doi: :10.1016/j.procbio.2006.04.001
587
588 Green, R., Su, T., Lu, J., Webster, J., & Penfold, J. (2000). Competitive adsorption of lysozyme
589 and C12E5 at the air/liquid interface. *Physical Chemistry Chemical Physics*, 2, 5222-
590 5229. doi: 10.1039/B004359L
591
592 Haskard, C. and Li-Chan, E. (1998). Hydrophobicity of Bovine Serum Albumin and Ovalbumin
593 determined using uncharged (PRODAN) and anionic (ANS-) fluorescent probes. *Journal*
594 *of Agricultural Food Chemistry*, 46, 2671-2677
595
596 Keymanesh, Soltani, & Sardari, (2009). Application of antimicrobial peptides in agriculture and
597 food industry. *World Journal of Microbiology and Biotechnology*, 25, 933–944. doi:
598 org/10.1007/s11274-009-9984-7
599
600 Lad, M., Birembaut, F., Frazier, R., & Green, R. (2005). Protein-lipid interactions at the air/water
601 interface. *Physical Chemistry Chemical Physics*, 7, 3478- 3485. doi: 10.1039/b506558p
602
603 Lad, M., Birembaut, F., Clifton, L., Frazier, R., Webster, J., & Green, R. (2007). Antimicrobial
604 peptide-lipid binding interactions and binding selectivity. *Biophysical Journal*, 92, 3575–
605 3586. doi: 10.1529/biophysj.106.097774
606
607 Lopez-Rubioa, A., & Gilbert, E. (2009). Neutron scattering: a natural tool for food science and
608 technology research. *Trends in Food Science and Technology*, 20, 576- 586.
609 doi:10.1016/j.tifs.2009.07.008
610
611 Manyi-Loh, C., Mamphweli, S., Meyer, E., & Okoh, A. (2018). Antibiotic use in agriculture and
612 its consequential resistance in environmental sources: potential public health
613 implications. *Molecules*, 23, 795; doi:103390/molecules23040795
614
615 Munita, J. & Arias, C. (2016). Mechanisms of antibiotic resistance. *Microbiology Spectrum*,
616 4(2). doi:10.1128/microbiolspec
617
618 Nakano, M.; Fukuda, M.; Kudo, T.; Endo, H.; Handa, T. (2007). Determination of Interbilayer
619 and transbilayer lipid transfers by time-resolved small-angle neutron scattering. *Physical*
620 *Review Letters*, 98. doi:238101-238104.
621

- 622 Nelson, A. (2006). Co-refinement of multiple-contrast neutron/X-ray reflectivity data using
623 MOTOFIT. *Journal of Applied Crystallography*, 39, 273–276. doi:
624 doi.org/10.1107/S002188980600507
625
- 626 Ohashi, Y. & Ushida, K. (2009). Health-beneficial effects of probiotics: Its mode of action.
627 *Animal Science Journal*, 80, 361–371 doi: 10.1111/j.1740-0929.2009.00645.x
628
- 629 Oliveira, R., Schneck, E., Quinn, B., Konovalov, O., Brandenburg, K., Seydel, U., Gill, T.,
630 Hanna, C., Pink, D., Tanaka, M. (2009). Physical mechanisms of bacterial survival
631 revealed by combined grazing-incidence X-ray scattering and Monte Carlo simulation.
632 *Chimie*, 12, 209-217. doi: 10.1016/j.crci.2008.06.020
633
- 634 Omardien, S., Brul, S., and Zaat, S. (2016). Antimicrobial activity of cationic antimicrobial
635 peptides against Gram-positives: current progress made in understanding the mode of
636 action and the response of bacteria. *Frontiers in Cell and Developmental Biology*, 4, 1-
637 16. doi.org/10.3389/fcell.2016.00111
638
- 639 Parisio, G., Ferrarini, A., and Sperotto, M. (2016). Model studies of lipid flip-flop in membranes.
640 *International Journal of Advances in Engineering Sciences and Applied Mathematics*, 8,
641 134–146. doi: 10.1007/s12572-015-0155-9
642
- 643 Pelegri, P., del Sarto, R., Silva, O., Franco, O., & Grossi-de-Sa, M. (2011). Antibacterial
644 peptides from plants: What they are and how they probably work. *Biochemistry Research*
645 *International*, 2011, 1-9. <http://dx.doi.org/10.1155/2011/250349>
646
- 647
- 648 Pink, D., Truelstrup Hansen, L., Gill, T., Quinn, B., Jericho, M., & Beveridge, T. (2003).
649 Divalent calcium ions inhibit the penetration of protamine through the polysaccharide
650 brush of the outer membrane of Gram-negative bacteria. *Langmuir*, 19, 8852–8858.
651 doi: 10.1021/la030193e
652
- 653 Pink, D., Hasan, F., Quinn, B., Winterhalter, M., Mohan, M., & Gill, T. (2014). Interaction of
654 protamine with Gram-negative bacteria membranes: possible alternative mechanisms of
655 internalization in *Escherichia coli*, *Salmonella Typhimurium* and *Pseudomonas*
656 *aeruginosa*. *Journal of Peptide Science*, 20, 240–250. doi: 10.1002/psc.2610
657
- 658 Pinto, M., Carvalho, A., Pires, S., Campus, A., Fonseca da Silva, H., Sobral, D., dePaula, J., &
659 de lima Santos, A. (2011). The effects of nisin on *Staphylococcus aureus* count and the
660 physicochemical properties of traditional Minas Serro cheese. *International Dairy*
661 *Journal*, 21, 90–96. doi: doi.org/10.1016/j.idairyj.2010.08.001
662
- 663 Potter, R., Truelstrup Hansen, L., & Gill, T. (2005). Inhibition of foodborne bacteria by native
664 and modified protamine: Importance of electrostatic interactions. *International Journal of*
665 *Food Microbiology*, 103, 23– 34. doi: 10.1016/j.ijfoodmicro.2004.12.019
666

667 Sanders, M., Clifton L., Frazier, R., and Green, R. (2016). Role of lipid composition on the
668 interaction between a tryptophan-rich protein and model bacterial membranes. *Langmuir*,
669 32, 2050–2057. doi: 10.1021/acs.langmuir.5b04628
670

671 **Sohlenkamp, C., & Geiger, O. (2016). Bacterial membrane lipids: diversity in structures and**
672 **pathways. *FEMS Microbiology Reviews*, 40, 133–159.**
673 **<https://doi.org/10.1093/femsre/fuv008>**
674

675 Spratt, B., Bowler, L., Zhang, Q., Zhou, J., & Smith, J. (1992). Role of interspecies transfer of
676 chromosomal genes in the evolution of penicillin resistance in pathogenic and commensal
677 *Neisseria* species. *Journal of Molecular Evolution*, 34:115-125. doi:
678 org/10.1007/BF00182388
679

680 **Straus, S. & Hancock, R. (2006). Mode of action of the new antibiotic for Gram-positive**
681 **pathogens daptomycin: Comparison with cationic antimicrobial peptides and**
682 **lipopeptides. *Biochimica et Biophysica Acta*, 1758, 1215–1223.**
683 **doi:10.1016/j.bbamem.2006.02.009**
684

685 Strömstedt, A., Ringstad, L., Schmidtchen, L., Malmsten, M. (2010). Interaction between
686 amphiphilic peptides and phospholipid membranes. *Current Opinion in Colloid and*
687 *Interface Science*, 15, 467–478. doi: org/10.1016/j.cocis.2010.05.006
688

689

690 **Suzuki, K., & Ando, T. (1972). Studies on protamine: XVII. The complete amino acid sequence**
691 **of clupeine YI. *Journal of Biochemistry*, 72, 1433– 1446.**
692
693

694 Truelstrup Hansen, L., Austin, J. & Gill, T. (2001). Antibacterial effect of protamine in
695 combination with EDTA and refrigeration. *International Journal of Food Microbiology*,
696 66, 149-161. doi: org/10.1016/S0168-1605(01)00428-7
697

698 Ueno, R. Fujita, Y., Yamamoto, M., & Kozakai, H. (1988). Multiplication inhibitor for *Bacillus*
699 *cerus*. European patent application, 0372091. *European Patent Office*, Great Britain.
700

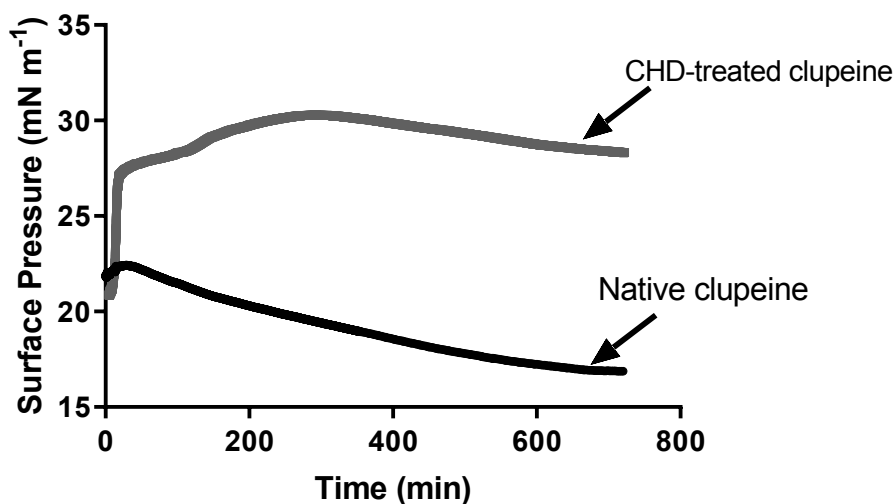
701 Vorobyov, I., & Allen, T. (2011). On the role of anionic lipids in charged protein interactions
702 with membranes. *Biochimica et Biophysica Acta*, 1808, 1673–1683.
703 doi.org/10.1016/j.bbamem.2010.11.009
704

705 Wu, M., Maier, E., Benz, R., & Hancock, R. (1999). Mechanism of interaction of different
706 classes of cationic antimicrobial peptides with planar bilayers and the cytoplasmic
707 membrane of the *Escherichia coli*. *Biochemistry*, 38, 7235–7242. doi: 10.1021/bi9826299
708

709

710

711
712
713
714
715
716



717

718 **Figure 1.** Surface pressure versus time plot for CHD-treated clupeine and native clupeine adsorbed
719 on a **PPC** monolayer. There was a general increase (4.6%) in surface pressure after adding the
720 CHD-treated peptide. On the other hand, the addition of the native peptide resulted in a decrease
721 (2.3%) in surface pressure. These experiments were repeated twice.

722

723 *Note that **PPC** is the abbreviation of PE:PG:CL.

724

725

726

727

728

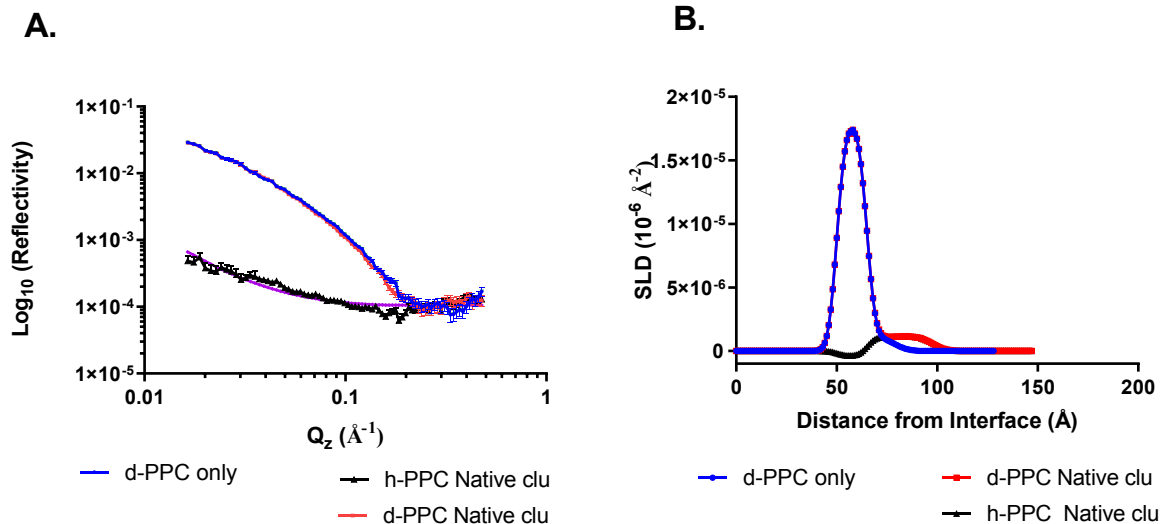
729

730

731

732

733



734

735 **Figure 2.** Neutron and X-ray reflectometry profiles and model data fits, and corresponding SLD
 736 profiles after equilibrium adsorption of native clupeine. (A) Reflectivity of **PPC** lipid monolayer
 737 in NRW with adsorbed native clupeine on the deuterated lipid in (red) and the hydrogenated lipid
 738 in (black) is plotted against $Q_z (\text{\AA}^{-1})$, the momentum transfer. The bare lipid with no peptide is
 739 shown in blue and the experimental data are represented with error bars whereas the best fit
 740 simulated data are represented as continuous lines. The SLD profile as a function of distance from
 741 the interface as determined from the fit is shown in (B).

742

*Note that **PPC** is the abbreviation of PE:PG:CL.

743

744

745

746

747

748

749

750

751

752

753

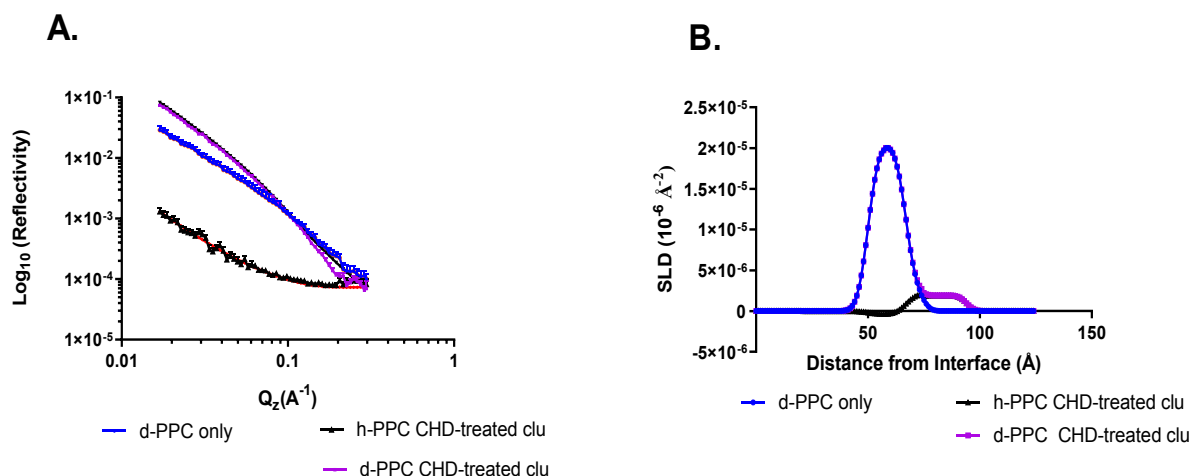
754

755

756

757

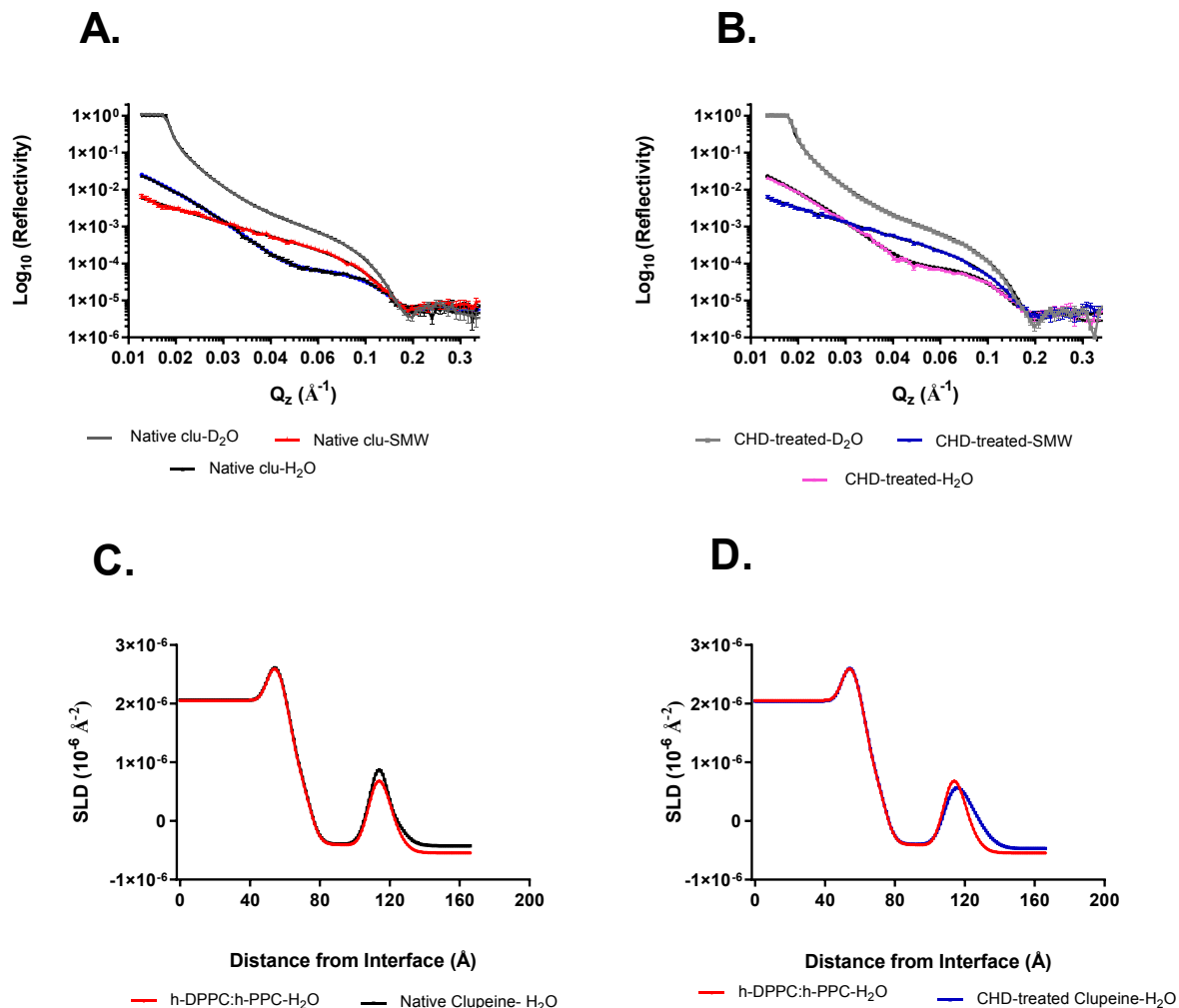
758



759
 760 **Figure 3.** Neutron and X-ray reflectometry profiles and model data fits, and corresponding SLD
 761 profiles after equilibrium adsorption of CHD-treated clupeine. (A) Reflectivity of PE:PG:CL
 762 monolayer in NRW with adsorbed CHD-treated clupeine on the deuterated lipid in (purple) and
 763 the hydrogenated lipid in (black). The bare lipid with no peptide is shown in blue and the
 764 experimental data are represented with error bars whereas the best fit simulated data are
 765 represented as lines. The SLD profile as a function of distance from the interface as determined
 766 from the fit is shown in (B).

767
 768 *Note that PPC is the abbreviation of PE:PG:CL.
 769

770
 771
 772
 773
 774
 775
 776
 777
 778
 779
 780
 781
 782
 783
 784



785
 786 **Figure 4.** Reflectivity curves and SLD profiles from d/h-DPPC:h-PPC lipid bilayer. **A.**
 787 Reflectivity data for the h-DPPC:h-PPC bilayer lipids in D₂O (gray), SMW (red), and H₂O (black)
 788 containing native clupeine. The corresponding fits are shown as lines, D₂O (black), SMW (black),
 789 and H₂O (blue). **B.** Reflectivity data for the h-DPPC:h-PPC bilayer lipids in D₂O (grey), SMW
 790 (blue), and H₂O (pink) containing CHD-treated clupeine. The fits are shown as black lines for all
 791 contrasts. **C.** SLD profiles for the bilayer in water contrast in the presence of native clupeine. The
 792 data are plotted as points with error bars and the fits are represented as a black line. SLD profile
 793 for bilayer in water contrast in the presence of CHD-treated clupeine. The data are plotted as points
 794 with error bars and the fits are represented as a blue line. The greater degree of hydration in the
 795 lipid head group region in the presence of CHD-treated clupeine compared to the native peptide is
 796 observed as a broader peak in Figure 4 D compared to Figure 4 C.

797 *Note that PPC is the abbreviation of PE:PG:CL.

798

799

800 **Table 1** Structural parameters obtained from the three layer model fits of native and CHD-
 801 treated clupeine (0.48 μM) adsorbed to **PPC** monolayers. The fits were repeated three times.

Parameters	Thickness τ (\AA)	SLD (10^{-6}\AA^{-2})	Layer roughness (\AA)	Γ Surface excess (mg/m^2)	(Φ_L) Lipid volume fraction
Layer 1, acyl chain					
d- PPC , NRW	15.0 \pm 0.01	1.60 \pm 0.01	3.51 \pm 0.15	0.005 \pm 0.02	0.59 \pm 0.02
h- PPC , NRW	15.0 \pm 0.01	-0.37 \pm 0.01			
h- PPC , XRR	15.0 \pm 0.01	9.69 \pm 0.03			
Layer 2, head group					
d- PPC , NRW	12.7 \pm 0.01	1.07 \pm 0.06		0.297 \pm 0.02	
h- PPC , NRW	12.7 \pm 0.01	1.07 \pm 0.06			
h- PPC , XRR	12.7 \pm 0.01	12.9 \pm 0.40			
Layer 3, peptide layer (native)					
d- PPC , NRW	15.3 \pm 0.07	1.00 \pm 0.09	3.88 \pm 0.32	0.364 \pm 0.02	
h- PPC , NRW	15.3 \pm 0.07	1.00 \pm 0.01			
h- PPC , XRR	15.3 \pm 0.07	10.9 \pm 0.01			
Layer 1, acyl chain					
d- PPC , NRW	16.5 \pm 0.14	2.08 \pm 0.05	3.83 \pm 0.06	0.007 \pm 0.03	0.69 \pm 0.03
h- PPC , NRW	16.5 \pm 0.14	-0.37 \pm 0.01			
h- PPC , XRR	16.5 \pm 0.14	8.64 \pm 0.01			
Layer 2, head group					
d- PPC , NRW	8.27 \pm 0.06	1.69 \pm 0.05		0.372 \pm 0.03	
h- PPC , NRW	8.27 \pm 0.06	1.69 \pm 0.05			
h- PPC , XRR	8.27 \pm 0.06	12.5 \pm 0.06			
Layer 3, peptide layer (CHD)					
d- PPC , NRW	17.6 \pm 0.05	1.42 \pm 0.44	3.50 \pm 0.44	0.59 \pm 0.14	
h- PPC , NRW	17.6 \pm 0.05	1.22 \pm 0.25			
h- PPC , XRR	17.6 \pm 0.05	9.25 \pm 0.05			

802 τ , represents layer thickness; Γ , represents, clupeine surface excess; and Φ_L represents lipid
 803 volume fraction

804 *Note that **PPC** is the abbreviation of PE:PG:CL.

805

806

807

808

809

810 **Table 2.** Best fit values and error estimates of asymmetrically deposited bare h-DPPC (inner
 811 leaflet) *E. coli* PPC (outer leaflet) bilayer deposited on a silicon surface and the bilayer in the
 812 presence of native and CHD-treated clupeine.
 813

Parameters of the Bilayer	Bare h-bilayer	h-bilayer + native clupeine	h-bilayer + CHD- treated clupeine
Oxide layer thickness (Å)	11.9 ± 2.6	nf	nf
Oxide layer hydration (%)	15.6 ± 2.4		
Oxide layer roughness (Å)	3.58 ± 0.95		
Inner head gp SLD (10 ⁻⁶ Å ⁻²)	1.53 ± 0.01	nf	nf
Inner head group hydration (%)	31.3 ± 5.5		
Inner head group thickness (Å)	11.9 ± 3.3		
Inner tail SLD (10 ⁻⁶ Å ⁻²)	-0.39	nf	nf
Inner tail hydration (%)	8.18 ± 1.5		
Inner tail thickness (Å)	15.7 ± 2.2		
Outer tail SLD (10 ⁻⁶ Å ⁻²)	-0.39	nf	nf
Outer tail hydration (%)	4.45 ± 0.93		
Outer tail thickness (Å)	19.2 ± 0.89		
Outer head gp SLD (10 ⁻⁶ Å ⁻²)	2.51 ± 0.30	2.17 ± 0.50	2.27 ± 0.48
Outer head group hydration (%)	17.9 ± 12.7	26.9 ± 5.5	48.2 ± 12
Outer head group thickness (Å)	7.94 ± 0.54	8.52 ± 0.04	8.13 ± 0.66
Bilayer roughness (Å)	4.99 ± 0.01	nf	nf
Clupeine hydration (%)	n.a.	48.8 ± 3.1	58.9 ± 15
Clupeine thickness (Å)	n.a.	4.15 ± 2.9	11.0 ± 6.0
Clupeine roughness (Å)	n.a.	3.15 ± 2.7	6.91 ± 1.6

814 nf = not fitted and n.a. = not applicable

815 *Note that PPC is the abbreviation of PE:PG:CL.

816

817

Appendix A

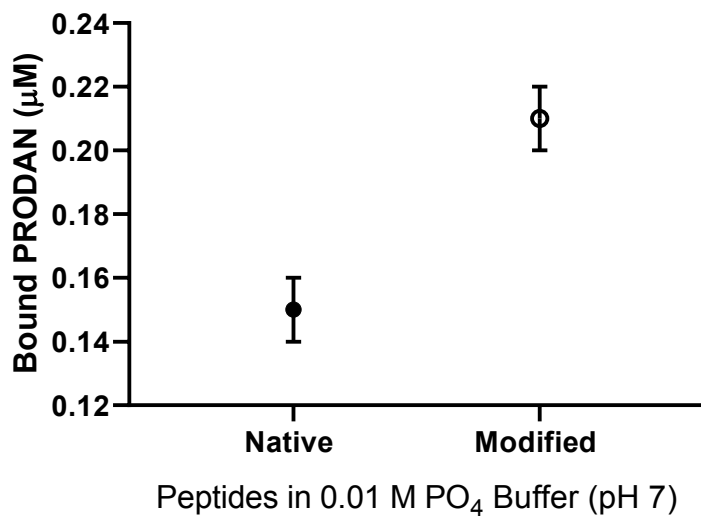


Figure 1A. The binding of PRODAN to native and modified clupeine. The surface hydrophobicity of the native and modified clupeine was measured using an uncharged probe, PRODAN. A PRODAN standard curve was developed which was used to measure the amount of probe bound to the clupeine samples.

Table A1. Summary of Scattering length scattering length densities, molecular weights, and molecular volumes of the lipids (PPC and DPPC) and peptides used in the present study.

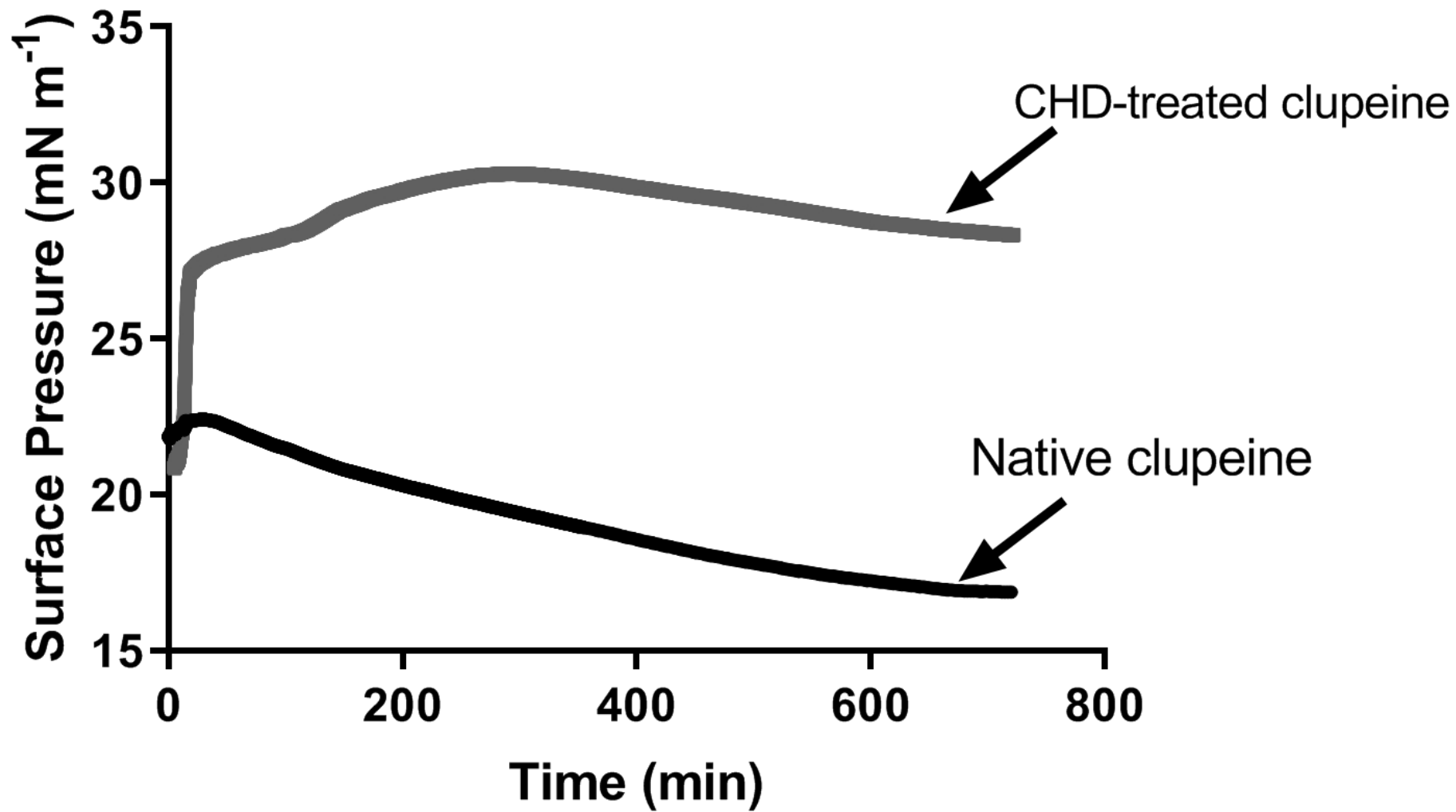
Parameters	Scattering length Σb (10^{-3}\AA)	SLD (10^{-6}\AA^{-2})	Molecular Weight (g/mol)	Molecular Volume (\AA^3)
h-PPC (head + tail)	0.339	0.300	720	1128
h-PPC (hd. group)	0.598	2.06	273	288
d-PPC tail	6.24	7.49	496	838
h-PPC tail	-0.326	-0.394	434	838
Native clupeine in NRW	29.0	2.02	4200	
CHD-treated clupeine in NRW	29.0	2.02	4200	
h-DPPC (head + tail)	0.277	0.241	734	1152
h-DPPC (hd. group)	0.597	1.74	311	342
h-DPPC tail		-0.39 ^a		
d-DPPC tail		7.45 ^a		

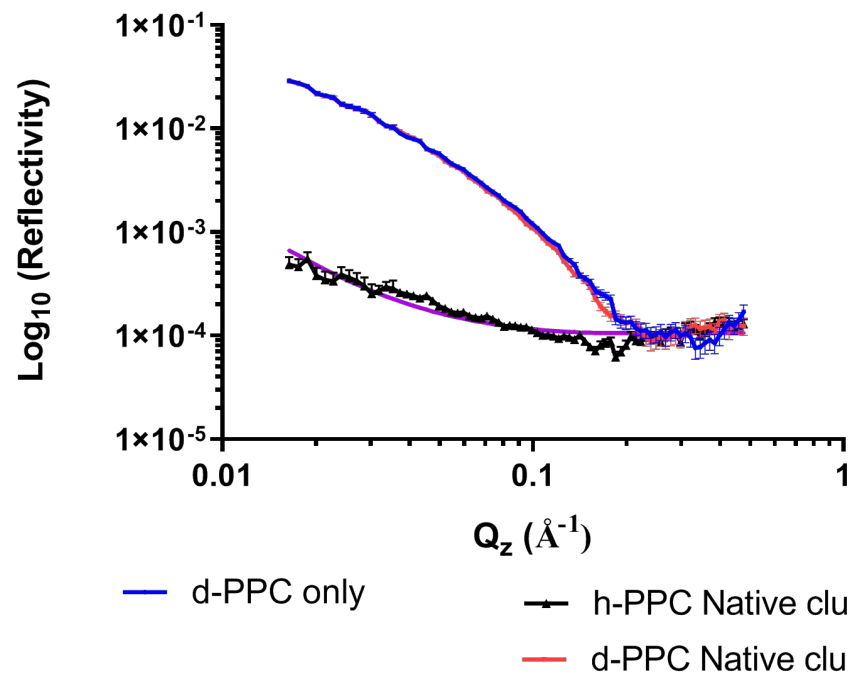
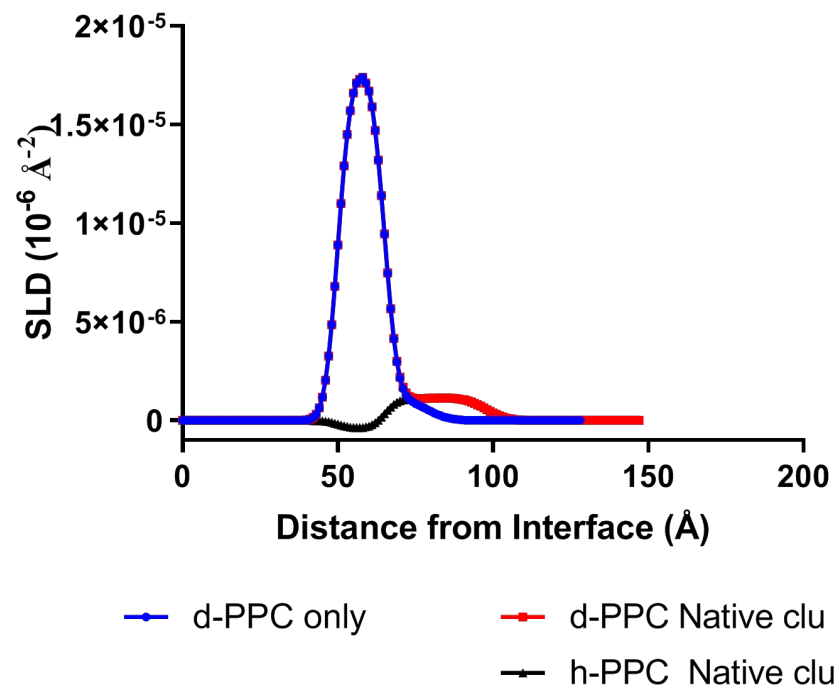
^a These values were obtained from Clifton et al. (2013 b).

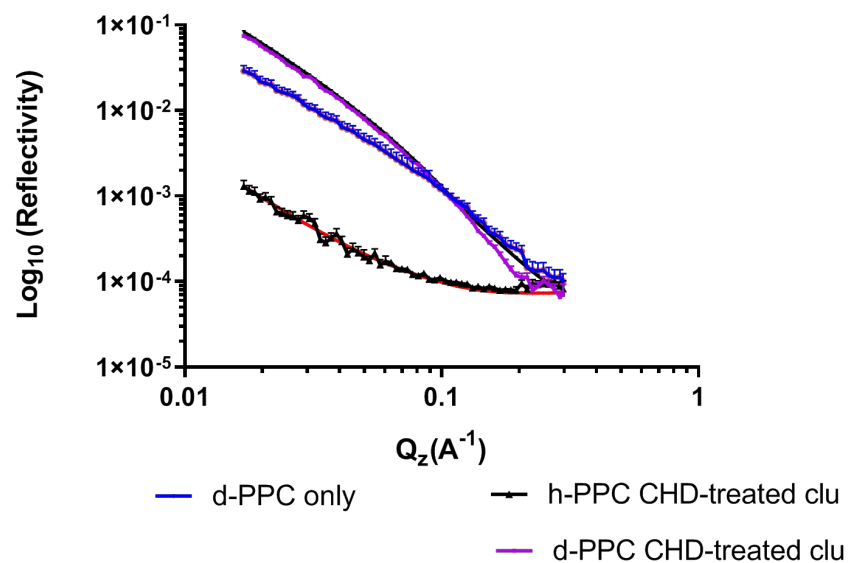
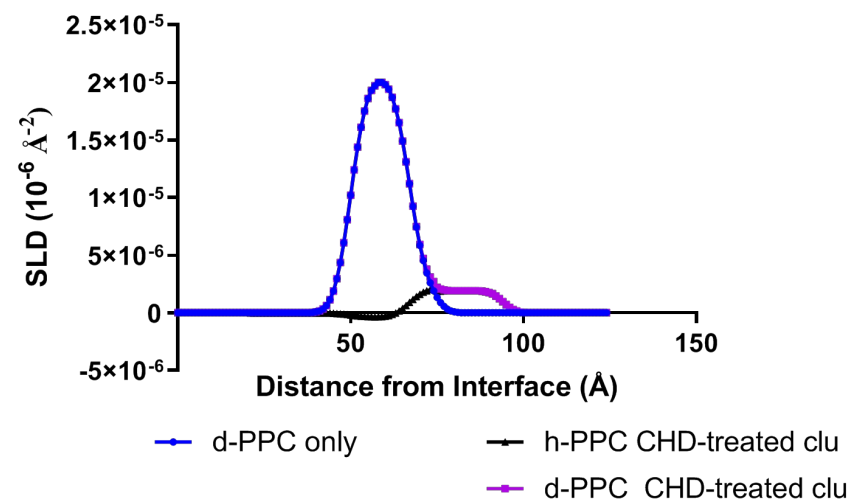
Table A2 Structural parameters obtained from a two-layer model fit of a condensed phase d-PE:PG:CL monolayer obtained from simultaneously fitting NR and XRR profiles. The structural parameters described for each layer are the layer thickness (τ), the SLD (ρ) and the corresponding layer roughness. The fits were repeated three times.

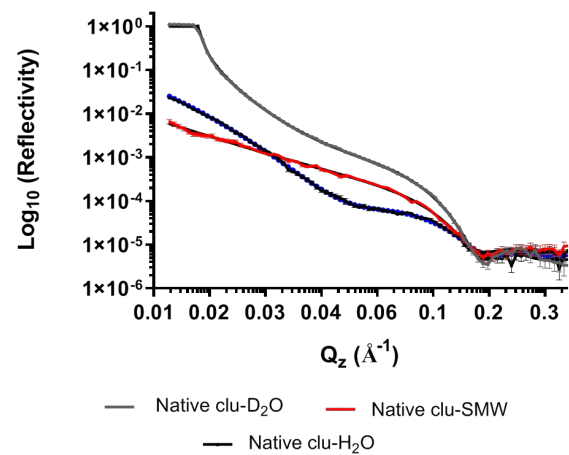
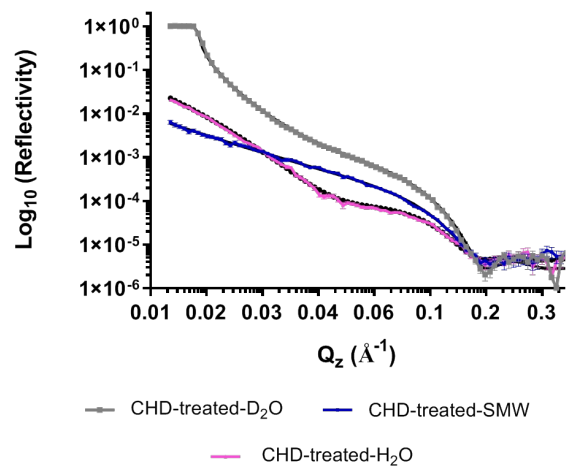
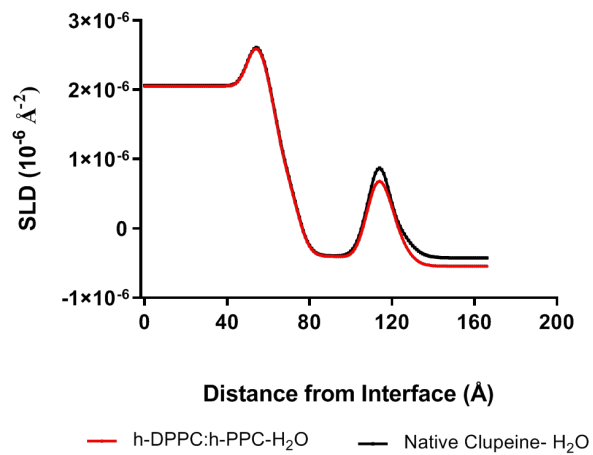
Parameters	Thickness τ (Å)	SLD (10^{-6}Å^{-2})	Layer roughness (Å)	Lipid volume fraction (Φ_L)
Layer 1, acyl chain				
d-PE:PG:CL, NR	15.0 ± 0.64	7.28 ± 0.76	3.93 ± 1.1	0.97 ± 0.02
h-PE:PG:CL, XRR	15.0 ± 0.64	9.55 ± 0.49		
Layer 2, head group				
d-PE:PG:CL, NR	12.9 ± 1.2	0.46 ± 0.25		
h-PE:PG:CL, XRR	12.9 ± 1.2	13.2 ± 0.07		

τ , represents layer thickness and Φ_L , represents lipid volume.



A.**B.**

A.**B.**

A.**B.****C.****D.**